Nonperiodic delay mechanism and fractallike behavior in classical time-dependent scattering

P. K. Papachristou,[1] F. K. Diakonos,[1] E. Mavrommatis,[1] and V. Constantoudis[2]
[1]*Department of Physics, University of Athens, Panepistimiopolis, 157 71 Athens, Greece*
[2]*Department of Physics, National Technical University, Zografou Campus, 157 80 Athens, Greece*
(Received 18 November 2000; revised manuscript received 13 February 2001; published 13 June 2001)

We study the occurrence of delay mechanisms other than periodic orbits in scattering systems with time-dependent potentials. By using as model system two harmonically oscillating disks on a plane, we have found the existence of a mechanism not related to the periodic orbits of the system, that delays trajectories in the scattering region. This mechanism creates a fractallike structure in the scattering functions and can possibly occur in several time-dependent scattering systems.

DOI: 10.1103/PhysRevE.64.016205 PACS number(s): 05.45.Pq

I. INTRODUCTION

Scattering processes are of fundamental importance in physical, chemical, and biological systems, because they can give insight into the characteristics of the scatterer. The majority of works in classical scattering has been focused on time-independent scattering. In this case the dynamics is classified into regular and chaotic according to the singularity structure of the corresponding scattering functions [1–4]. Regular scattering is associated with smooth scattering functions with a finite number of singularities. On the contrary, chaotic scattering functions are characterized by a fractal set of singularities. A typical representative of regular scattering is a system consisting of two static disks on a plane [5], whereas the addition of a third disk in a triangular configuration leads to chaotic scattering [6].

Time-dependent classical scattering has received less attention. Rich dynamical behavior is expected in some of the cases as it has been recently observed in Refs. [7–15] but there is still a lack of a deeper understanding of the processes involved. In the present work we also address the problem of classical scattering off a time-dependent scatterer, focusing on the question how the time dependence influences the dynamics in the scattering region. In order to isolate the effects of time dependence, we consider the time-dependent counterpart of the above-mentioned *integrable* system consisting of two static disks on a plane. The main advantage of this system is that choosing an appropriate set of initial conditions we can eliminate the effects of the bounded orbits of the system on the scattering dynamics. Thus we can illuminate delay mechanisms other than the traditional ones based on the presence of chaotic invariant sets of unstable periodic orbits. The time dependence in our system is introduced by assuming that the two disks oscillate harmonically with time. A similar system has also been studied by Antillón *et al.* [14] using, however, a nonharmonic oscillation law. It is found that the time dependence gives rise to a complicated fractallike behavior in the scattering functions resembling the rich structure observed in static chaotic scattering: as opposed to the regular case, discontinuities are found to occur at many different scales. However, the structure of these discontinuities is not self-similar at arbitrarily small scales. This uneven behavior is related to a nonperiodic delay mechanism, based on a large energy loss of the scattered particle and not to the presence of phase-space structures which trap the particle in the scattering region. Nonperiodic delay processes have also been reported in the literature [13]. Nevertheless, in that case a bounded chaotic set containing infinitely many aperiodic trajectories is responsible for the delay. Our study could serve as a first step towards the deeper understanding of certain scattering processes off oscillating targets, such as molecules, atomic clusters, surfaces, and nuclei in the cluster model.

The outline of the paper is as follows: In Sec. II we introduce our model. In Sec. III we present the results of our numerical investigations. In Sec. IV we attempt to give an interpretation of the above results by identifying the mechanism that leads to the delay of the trajectories in the scattering region. In Sec. V we summarize our main results and comment on the possible extensions of this work.

II. DESCRIPTION OF THE MODEL

We consider the scattering of a free point particle off two circular harmonically oscillating disks on a plane, as shown in Fig. 1. The disks are considered to be much heavier than the scattered particle. The recoil of the disks at the collision

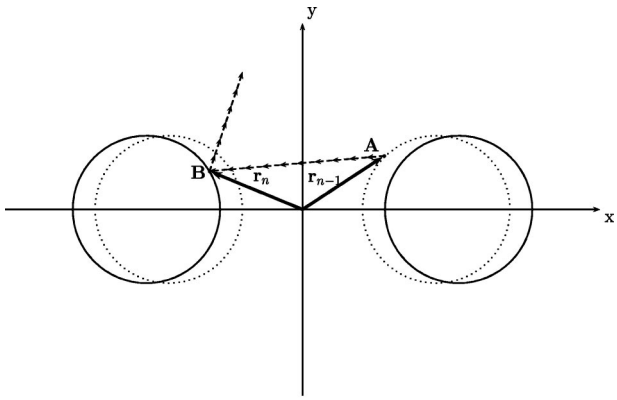

FIG. 1. The two oscillating disks on the x-y plane. The positions of disks at time t_{n-1} are drawn with the dotted line and at t_n with the solid line. The point A, which is defined with the vector $\mathbf{r}_{n-1}$, is the point of the $(n-1)$th bounce. The point B, which is defined with $\mathbf{r}_n$, is the point of the nth bounce. The dashed line with the arrows represents a segment of a trajectory that bounces between the two disks.

is not taken into account and therefore the total energy of the system is not conserved. The centers of the disks are oscillating harmonically along the same axis. The position of the center of the ith disk is given by the equation

$$\mathbf{d}_i(t)=\mathbf{d}_i^{(0)}+\mathbf{A}_i\sin(\omega_i t+\phi_i), \tag{1}$$

where $\mathbf{d}_i^{(0)}$ denotes the equilibrium position of the center, $\mathbf{A}_i$ is a vector directed along the axis of oscillation having magnitude equal to the amplitude of the oscillation, ω_i is the angular frequency of the oscillation, and ϕ_i is the initial phase. The position $\mathbf{r}(t)$ and the velocity $\mathbf{u}(t)$ of the particle in the time interval between the $(n-1)$th and the nth bounce are given by

$$\mathbf{r}(t)=\mathbf{r}_{n-1}+(t-t_{n-1})\mathbf{u}_{n-1},$$

$$\mathbf{u}(t)=\mathbf{u}_{n-1}, \tag{2}$$

where $\mathbf{r}_{n-1}$ denotes the position of the $(n-1)$th bounce, $\mathbf{u}_{n-1}$ denotes the velocity of the scattered particle after the $(n-1)$th bounce, and t_{n-1} denotes the time when that bounce occurred. In order to find the time t_n when the next bounce will occur, we must solve the equation

$$\|\mathbf{d}_i(t)-\mathbf{r}(t)\|^2=R_i^2, \tag{3}$$

where R_i denotes the radius of the ith disk. This equation must be solved twice (for $i=1,2$) and the smallest nonnegative solution has to be kept. The condition (3) leads to the equation

$$c_1(t-t_{n-1})^2+c_2\sin^2(\omega_i t+\phi_i)+c_3(t-t_{n-1})\sin(\omega_i t+\phi_i)+c_4(t-t_{n-1})+c_5\sin(\omega_i t+\phi_i)+c_6=0, \tag{4}$$

where the coefficients $c_1,\ldots,c_6$ are given by

$$c_1=\mathbf{u}_{n-1}^2,$$

$$c_2=\mathbf{A}_i^2,$$

$$c_3=-2\mathbf{u}_{n-1}\cdot\mathbf{A}_i,$$

$$c_4=2(\mathbf{r}_{n-1}-\mathbf{d}_i^{(0)})\cdot\mathbf{u}_{n-1}, \tag{5}$$

$$c_5=2(\mathbf{r}_{n-1}-\mathbf{d}_i^{(0)})\cdot\mathbf{A}_i,$$

$$c_6=(\mathbf{r}_{n-1}-\mathbf{d}_i^{(0)})^2-R_i^2.$$

Equation (4) is solved numerically to obtain t_n. Using Eq. (2), the position of the next bounce is then given by

$$\mathbf{r}_n=\mathbf{r}_{n-1}+(t_n-t_{n-1})\mathbf{u}_{n-1}. \tag{6}$$

Since the mass of the disks is considered to be much larger than that of the scattered particle, the velocity of the particle after the nth bounce is given by

$$\mathbf{u}_n=\mathbf{u}_{n-1}-2[\mathbf{n}\cdot(\mathbf{u}_{n-1}-\mathbf{V}_i)]\cdot\mathbf{n}, \tag{7}$$

where $\mathbf{n}$ is the normal to the disk at the point of the impact and $\mathbf{V}_i$ is the velocity of the involved disk at the instant of the collision, which is given by

$$\mathbf{V}_i=\mathbf{A}_i\omega_i\cos(\omega_i t_n+\phi_i). \tag{8}$$

In our study we have chosen the x axis as the axis of oscillation [$\mathbf{A}_i=(A_i,0)$]. We have also chosen the radii, the angular frequencies, and the amplitudes of the disks to be the same ($R_1=R_2=R$, $\omega_1=\omega_2=\omega$, $A_1=A_2=A$). Equations (6) and (7) are invariant under the scaling transformation

$$\omega\to\lambda\omega,\quad \mathbf{u}_n\to\lambda\mathbf{u}_n,\quad t_n\to\frac{t_n}{\lambda}, \tag{9}$$

and therefore the system can be described in terms of the dimensionless variables

$$\tilde{\mathbf{u}}_n=\frac{\mathbf{u}_n}{A\omega},\quad \tilde{t}_n=\omega t_n,\quad \tilde{\mathbf{r}}_n=\frac{\mathbf{r}_n}{A}. \tag{10}$$

By following the above procedure, we iterate numerically the map $(\tilde{\mathbf{r}}_n,\tilde{\mathbf{u}}_n,\tilde{t}_n)\to(\tilde{\mathbf{r}}_{n+1},\tilde{\mathbf{u}}_{n+1},\tilde{t}_{n+1})$ and obtain the trajectories for a large number of initial conditions.

III. NUMERICAL RESULTS

A. Fractallike scattering functions

The scattering region is defined as a circular domain of radius $R_0>R_i$ centered at the origin. As initial conditions we choose $\tilde{\mathbf{r}}(0)=0$ and $\tilde{\mathbf{u}}(0)=(\tilde{u}_0\cos\alpha,\tilde{u}_0\sin\alpha)$. For the majority of our numerical calculations we have chosen the dimensionless parameters of the system to be $\tilde{R}=R/A=10$, $\tilde{\mathbf{d}}_1^{(0)}=\mathbf{d}_1^{(0)}/A=(-15,0)$, $\tilde{\mathbf{d}}_2^{(0)}=\mathbf{d}_2^{(0)}/A=(15,0)$, $\phi_1=\pi$, $\phi_2=0$, $\alpha=10^{-2}$ rad, and $\tilde{R}_0=100$. For these values of the parameters the scattered particle exhibits a small number of bounces (typically 4–7), in contrast to Ref. [14] where the number of bounces is much larger (typically more than 100) due to the different choice of the parameters. We have obtained the delay time $\tilde{T}$ that the particle spends in the scattering region, the scattering angle ϕ_{out}, and the outgoing velocity $\tilde{u}_{out}$ as a function of $\tilde{u}_0$. The results are shown in Fig. 2. A rich fractallike structure is observed in these scattering functions for rather small values of $\tilde{u}_0$. As $\tilde{u}_0$ increases, the scattering functions become more regular. In order to study the dependence of the structure of this function on the angle α, we have calculated $\tilde{T}(\tilde{u}_0)$ for $\alpha=10^{-3}$ rad and $\alpha=10^{-1}$ rad. The results are shown in Fig. 3. We observe that as the angle increases the function becomes more regular in the sense that the range of $\tilde{u}_0$ in which $\tilde{T}(\tilde{u}_0)$ exhibits wild oscillations becomes smaller. This was expected since for smaller α the particle exhibits more bounces and therefore senses more strongly the dynamics in the scattering region. We observe that the peak structure of $\tilde{T}(\tilde{u}_0)$ behaves as a fractal set for many different scales. The lower limit where the breaking of the fractality occurs becomes smaller and smaller as we approach the region $\tilde{u}_0\to 0$. In

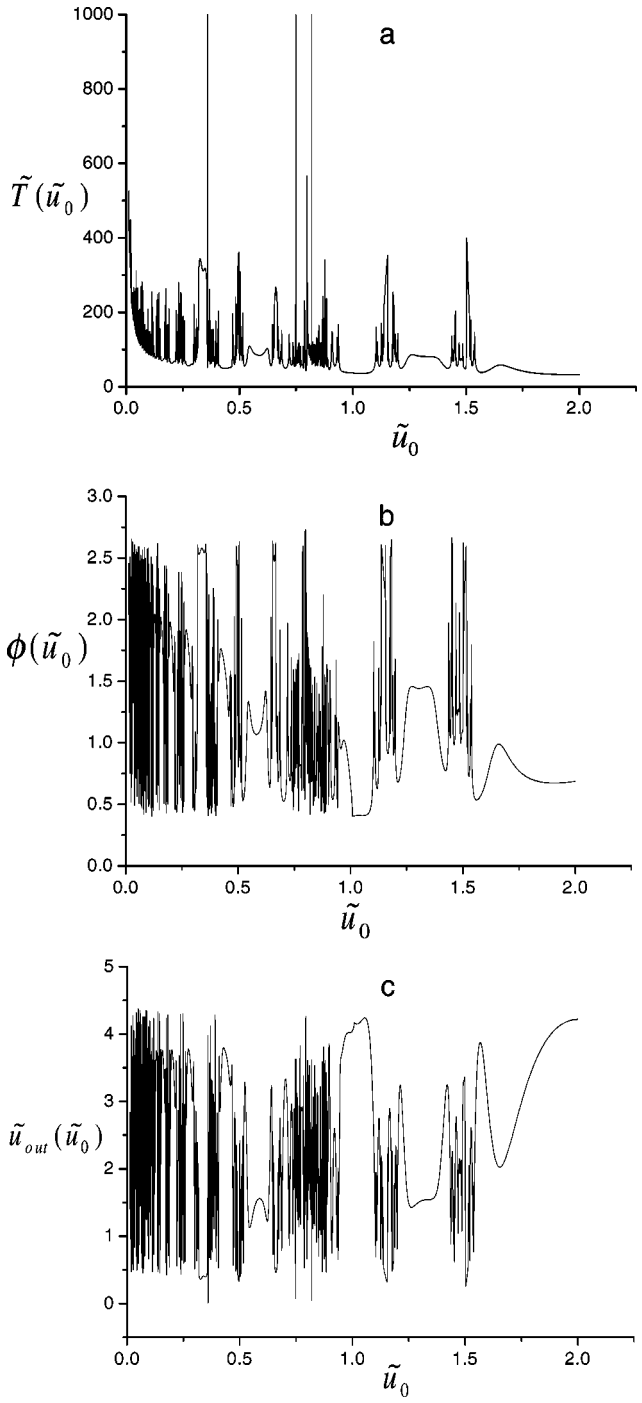

FIG. 2. (a) The delay time $\tilde{T}$, (b) the scattering angle ϕ_{out} (in radians), and (c) the outgoing velocity $\tilde{u}_{out}$ as a function of the initial velocity $\tilde{u}_0$ for initial angle $\alpha = 10^{-2}$ rad. All the plots were created by iterating 10^4 initial conditions.

order to investigate the apparent fractal structure of the system, we make successive magnifications of the $\tilde{T}(\tilde{u}_0)$ plot of Fig. 2(a) in a region of $\tilde{u}_0$ around the value 0.8. The results are shown in Fig. 4. We observe that the fractallike structure breaks at a very small scale. In this $\tilde{u}_0$ region, this breaking scale is found to be around 10^{-7}. In the following, a more in depth analysis of these findings will be given.

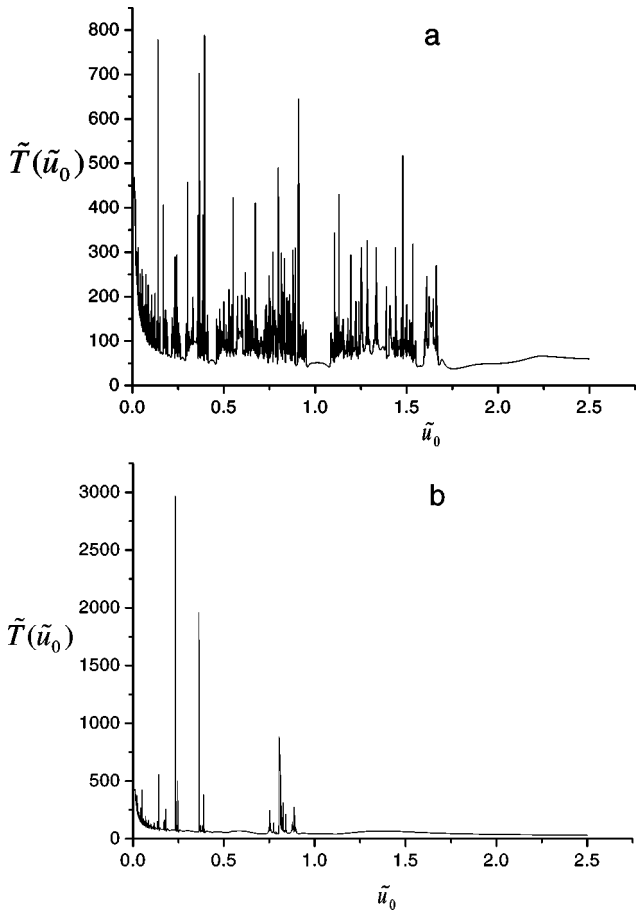

FIG. 3. The delay time $\tilde{T}$ as a function of the initial velocity $\tilde{u}_0$ for the values of the initial angle α (a) $\alpha = 10^{-3}$ rad, (b)$\alpha = 10^{-1}$ rad.

B. Investigation of the fractallike structure

In order to quantify the observations concerning the apparent fractality of the system made in the previous subsection, we have calculated an effective uncertainty dimension of $\tilde{T}(\tilde{u}_0)$ [16,17]. The uncertainty dimension is given by $d_u = 1 - \beta$, where β appears as $f(\epsilon) \approx \epsilon^{\beta}$ at the $\epsilon \to 0$ limit. $f(\epsilon)$ is the fraction of uncertain points, for a given value of uncertainty, ϵ, and for randomly chosen points $\tilde{u}_0$. Each $\tilde{u}_0$ is considered to be uncertain if we find that the difference $|T(\tilde{u}_0) - T(\tilde{u}_0 + \epsilon)|$ is larger than a number of order 1. ϵ cannot tend to zero since we have found that our system is not self-similar at arbitrarily small scales. We therefore use the term effective dimension to indicate the slope of $\log f(\epsilon)$ vs $\log \epsilon$ in a finite range of ϵ. In our calculation we have included as many random points as necessary to obtain 150 uncertain points per run. We have calculated the effective uncertainty dimension for several values of α and in all cases $\log f(\epsilon)$ as a function of $\log \epsilon$ can be well fitted by a straight line, indicating that the system resembles the behavior of a fractal at many different scales. A plot of $\log f(\epsilon)$ as a function of $\log \epsilon$ for $\alpha = 10^{-2}$ rad is shown in Fig. 5. The corresponding effective dimension is found to be equal to 0.58. The effective dimensions are not sensitive to variations of

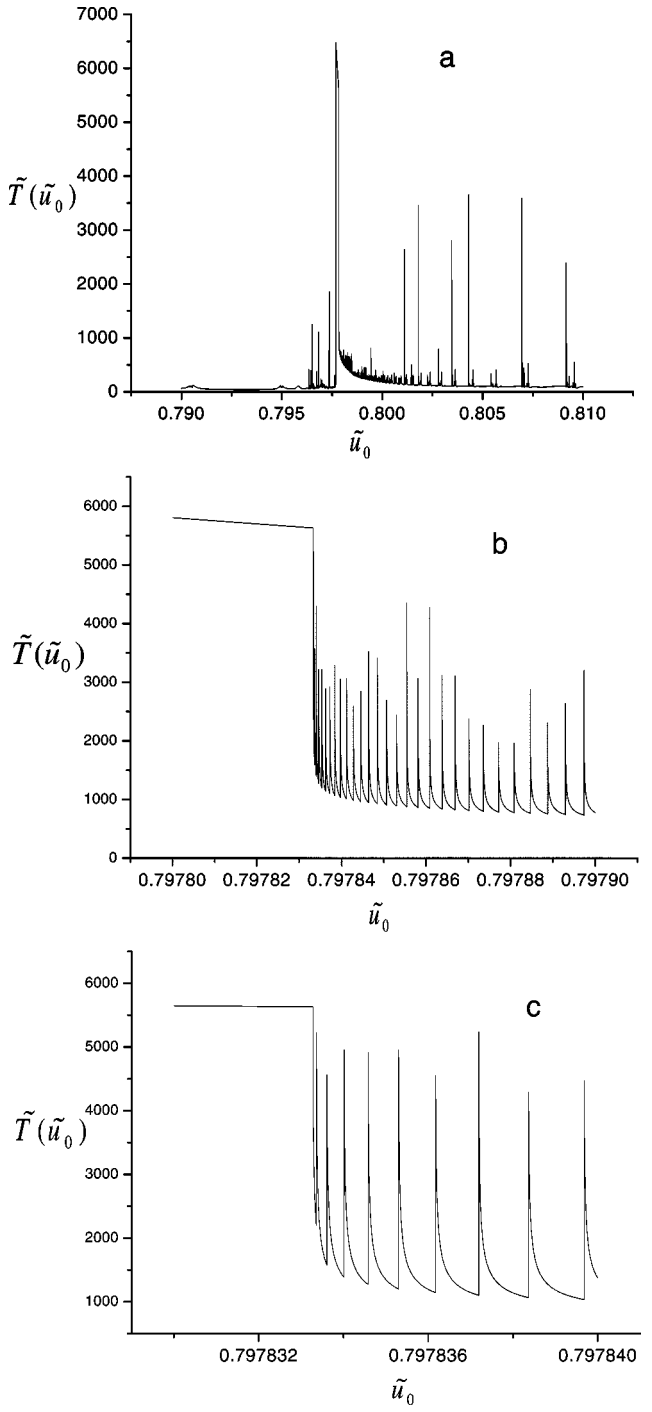

FIG. 4. Magnifications of Fig. 2(a) around the value 0.8 of the initial velocity $\tilde{u}_0$. Although in (a) a self-similar structure appears to exist, it is found that this structure does not persist at arbitrarily small scales as shown in (b) and (c).

the initial angle α: a variation of d_u of less than 10% is observed for a variation of α between the values 10^{-3} rad and 10^{-1} rad. For each angle α, there is a scale below which it is not possible to find any uncertain points. This supports our observation that self-similarity does not persist at arbitrarily small scales.

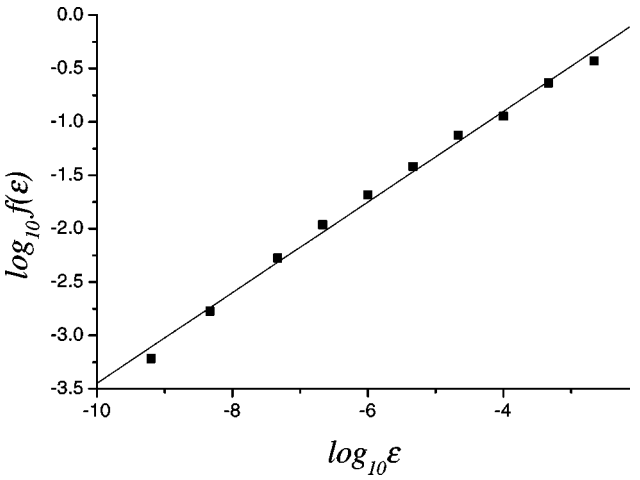

FIG. 5. The logarithm of the fraction of uncertain points $\log_{10}f(\epsilon)$ as a function of $\log_{10}\epsilon$ for $\alpha=10^{-2}$ rad. The fit with a straight line is also shown.

C. Decay law

We have also investigated the behavior of the function $N(t)/N_0$ which gives the fraction of particles that remain in the scattering region after time t. It is known that for hyperbolic systems $N(t)/N_0$ decays exponentially whereas for systems with marginal orbits and KAM tori it usually obeys a power law [18]. In order to study numerically the behavior of $N(t)/N_0$ we need to perform a Monte Carlo simulation by iterating a large number N_0 of randomly selected initial conditions. In our system, in contrast to the static two-disk system, an averaging over the initial velocity of the particle has also to be performed since the system is not conservative. In our calculation for the oscillating system, $\tilde{u}_0$ is uniformly distributed in $(0,2]$ since this is the range of $\tilde{u}_0$ where all the peaks of $\tilde{T}(\tilde{u}_0)$ occur. The angle α has been chosen in $(0,0.7]$ since for values of α in this range the particle exhibits at least one collision before exiting the scattering region. An averaging over the initial phases has also been performed. We have used 10^7 orbits. For some orbits the major loss of energy occurs at the last collision. These orbits escape from the scattering region with a very low velocity and therefore they correspond to pronounced peaks in the $\tilde{T}(\tilde{u}_0)$ plot. In order for these peaks not to be much higher than those corresponding to a delay of the particle between bounces, we choose $\tilde{R}_0=25$. The result is shown in Fig. 6. From this figure it is clear that for our system $N(t)/N_0$ is very close to a power law with an exponent which for the chosen values of the parameters is found to be approximately equal to -2.38. The corresponding static system is expected to have an exponential decay law. In this case, no averaging in u_0 is performed since the system is conservative. If we average in u_0 for the static system we will also obtain a power law with an exponent equal to -2 (the derivation is shown in the Appendix). If, on the other hand, we exclude from our calculations the ''uncertain'' trajectories [for which

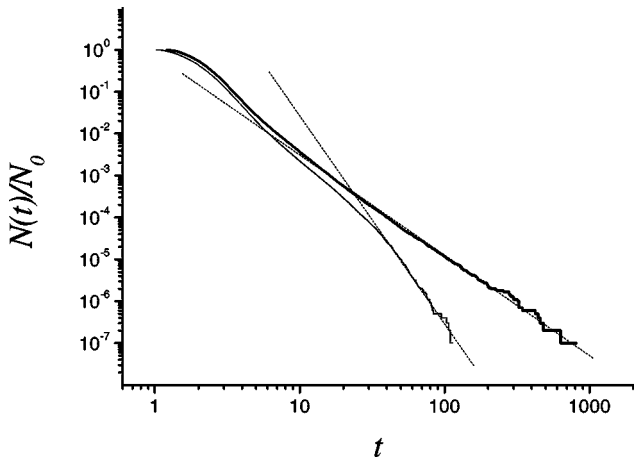

FIG. 6. The fraction $N(t)/N_0$ of particles remaining in the scattering region at time t. The thick solid curve includes all the trajectories and the thin solid curve includes only the ''certain'' trajectories (see Sec. III B). For large t both curves approximately obey power laws with different exponents. The dashed lines show the corresponding linear fits. The plots were created by iterating $N_0 = 10^7$ initial conditions.

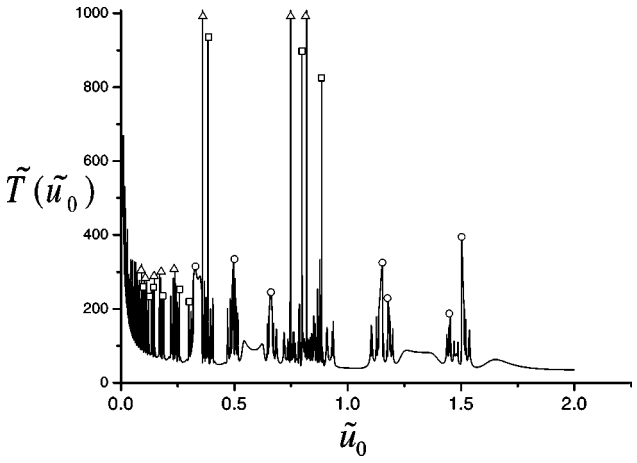

FIG. 7. Some of the major peaks of Fig. 2(a) are classified according to the bounce that leads to the major energy loss of the scattered particle. The symbols △, □, and ○ denote the first, the second, and the third bounce, respectively.

$|\tilde{T}(\tilde{u}_0,\phi,\alpha)-\tilde{T}(\tilde{u}_0+\epsilon,\phi,\alpha)|$ is larger than a number of order 1] for the oscillating system we find a decay which for large times follows approximately a power law with an exponent greater (in absolute value) than 2.38. It turns out that $\epsilon \approx 10^{-6}$ is an optimal value allowing the almost complete elimination of the peaks in $\tilde{T}(\tilde{u}_0)$ without deforming the background. For this value of ϵ we find an exponent approximately equal to -5. The result is shown in Fig. 6. From the above it becomes clear that although the presence of the oscillation accelerates the escape of the particles, the presence of the high peaks in the $\tilde{T}(\tilde{u}_0)$ function (uncertain points) introduces a delay of the particles and slows down the escape. The origin of these peaks will be discussed in the following section.

IV. INTERPRETATION OF THE RESULTS: A DIFFERENT DELAY MECHANISM

By analyzing the trajectories that stay for long times in the scattering region, we found that these do not exhibit a large number of bounces. The observed delay comes from orbits along which the scattered particle loses much of its energy and therefore traverses segments of its orbit with a very low velocity. This sudden loss of energy can happen at any of the bounces provided that $\|\mathbf{u}_{n-1}-2\mathbf{V}_i\|$ is small but not as small as for the particle to bounce on the same disk again. We have classified the peaks of the $\tilde{T}(\tilde{u}_0)$ plot according to the bounce which leads to the major loss of energy. The result is shown in Fig. 7. Prominent peaks that are due to the first bounce are observed. We also observe that around each of the peaks there is a rich fractallike structure. In the following we are going to give a qualitative interpretation of the above observations by using a simple one-dimensional model which neglects the curvature of the disks. This model can yield quantitative results only for the first and the second bounce, since with the parameters chosen, the scattered particle senses strongly the curvature of the disks after the second bounce.

Setting $\alpha=0$ the dynamics is limited to one spatial dimension. In this case the system resembles to the Fermi acceleration model [19,20]. For notational convenience we switch to the variables ω, $\mathbf{u}_n$, t_n [see Eq. (9)]. The particle starts at the origin with initial velocity $\mathbf{u}(0)=(u_0,0)$. In order to find the time t_c when the first collision with the right disk occurs, we have to solve the equation

$$u_0 t = \frac{D}{2} - R + A\sin(\omega t). \tag{11}$$

The time t_c can be thought of as the abscissa of the first point of intersection of the straight line $u_0 t$ with the sinusoidal curve $D/2-R+A\sin(\omega t)$ (see Fig. 8). From this figure it is obvious that t_c is a discontinuous function of u_0. Discontinuities occur for the values of u_0 for which the line is tangent to the sinusoidal curve. If we denote as t_c^+ the value of t_c after the discontinuity, the value of $u_0=u_0^*$ at which the discontinuity occurs is given by

$$u_0^* = A\omega\cos(\omega t_c^+). \tag{12}$$

Therefore the velocity of the particle after the first collision u_1 is also discontinuous as a function of u_0. At this point we should stress that the oscillation law need not only be harmonic for these discontinuities to occur. In Fig. 9(a) a plot of u_1 as a function of u_0 is shown. We observe sharp peaks that get denser as $u_0 \to 0$. For $u_0 \to 0$, the initial velocity that corresponds to a given t_c is given by

$$u_0 \cong \frac{\frac{D}{2}-R-A}{t_c}. \tag{13}$$

Therefore the distance between two successive peaks on the u_0 axis is given by

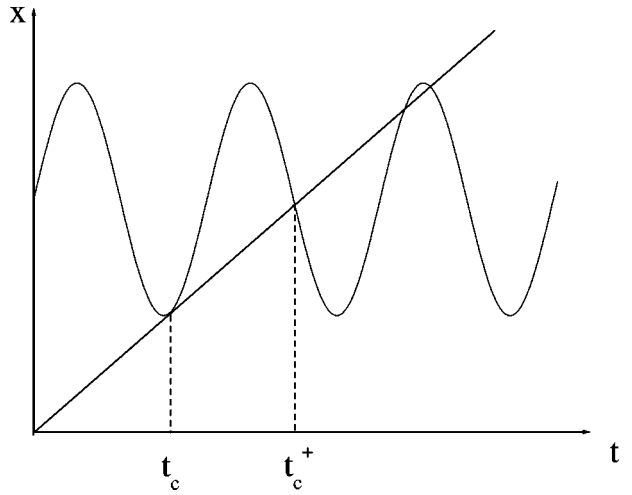

FIG. 8. The abscissa of the point of intersection of the sinusoidal curve $D/2-R+\sin\omega t$ and the straight line $u_0 t$ is the time t_c when the first bounce occurs for the one-dimensional system ($\alpha=0$). The slope of the straight line is u_0. For values of u_0 for which the straight line is tangent to the sinusoidal curve, t_c is discontinuous as a function of u_0. The value of t_c after the discontinuity is denoted as t_c^+.

$$\Delta u_0 \cong \frac{\frac{D}{2}-R-A}{t_c^2}\Delta t_c, \tag{14}$$

where $\Delta t_c \cong 2\pi/\omega$. Combining the above two relations, we conclude that $\Delta u_0 \sim u_0^2$ as $u_0 \to 0$. The density of the peaks therefore increases as $1/u_0^2$ as $u_0 \to 0$.

We observe that u_1 gets close to 0 near the discontinuities ($u_0 \cong 2V$, where V is the velocity of the disk involved in the collision). If the velocity after the collision is small, but not small enough as for the particle to rebounce on the same disk, there is a delay of the particle between the first and the second bounce. We expect this delay to be present in the original system ($\alpha \neq 0$) and to manifest itself as a peak in the $\tilde{T}(\tilde{u}_0)$ plot, since for small α the curvature of the disks can be neglected for the first collision.

In the following we will give a qualitative interpretation of the fact that there is a rich fractallike structure around the peaks of $\tilde{T}(\tilde{u}_0)$ for the original system. The quantity $|1/u_n|$ is a measure of how much time is spent between the nth and $(n+1)$th collision for the one-dimensional system. In Fig. 9(b) a plot of $|1/u_1|$ as a function of u_0 for the one-dimensional system is shown. We observe that the peaks of this plot are very close to the peaks of the $\tilde{T}(\tilde{u}_0)$ plot (Fig. 2) that correspond to the delay of the particle between the first and the second bounce. The $\tilde{T}(\tilde{u}_0)$ plot can be thought of as several iterations of $|1/\tilde{u}_n|$ plots which are expected to have a structure similar to the $|1/\tilde{u}_1|$ plot. For $\tilde{u}_0$ that corresponds to a peak of the $\tilde{T}(\tilde{u}_0)$ plot, $\tilde{u}_1$ falls in the low velocity region, where the structure of the $|1/\tilde{u}_1|$ plot is very dense. We therefore expect fingerprints of this dense structure to be apparent around any $\tilde{u}_0$ value which maps onto the low velocity region after some bounce. Since there is a lower bound on the velocity with which the particle can leave a disk, we do not expect the structure around the peaks to be infinitely dense. This is consistent with our observation that the fractal structure of $\tilde{T}(\tilde{u}_0)$ breaks at some small $\tilde{u}_0$ scale. The higher a peak of the $\tilde{T}(\tilde{u}_0)$ plot is, the smaller the velocity of the particle along the orbit and the lower the breaking scale. The above mechanism also explains the presence of peaks in the scattering functions of Ref. [14], however, the structure there is more dense due to the different choice of the parameters. Furthermore, the mechanism is also present when the oscillating hard disks are replaced by two oscillating potential hills. A detailed analysis of the dynamics of such a system is left for a future study.

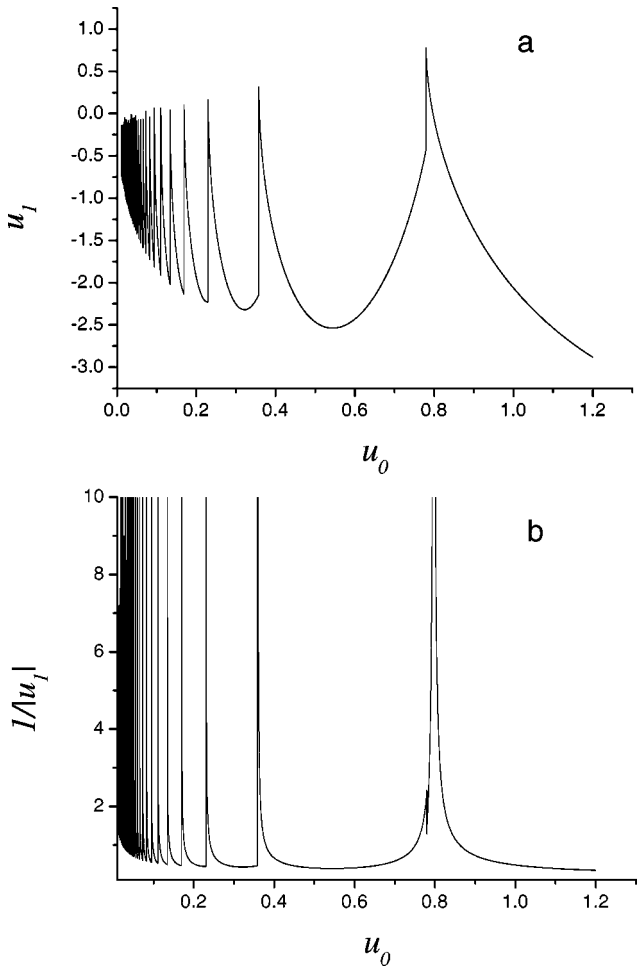

FIG. 9. (a) The velocity u_1 after the first bounce as a function of the initial velocity u_0 for the one-dimensional system ($\alpha=0$). (b) $|1/u_1|$ as a function of u_0 for the one-dimensional system. The locations of the singularities are very close to the locations of the peaks of Fig. 7 that correspond to a loss of energy of the scattered particle at the first bounce.

V. CONCLUSIONS AND OUTLOOK

In the present paper we have studied the effects of time dependence on the scattering process of a point particle off two harmonically oscillating hard disks. A different mecha-

nism leading to long-lived scattering trajectories has been found. It is associated with the energy loss of the scattered particle at the collisions. This mechanism is not directly related to the periodic orbits of the system and induces a fractallike structure in the scattering functions. At the statistical level, the mechanism manifests itself as a change in the properties of the fraction $N(t)/N_0$ of particles that remain in the scattering region after time t. Although this function still obeys a power law, the absolute value of the corresponding exponent is modified by a significant amount. An interesting question that will be studied in the future is how time dependence affects the dynamics of a system whose static counterpart is chaotic, such as the three disk system [6]. As an extension to this work, the transport properties of a lattice gas consisting of oscillating disks will be studied. Another open question is the quantum manifestation of this mechanism.

ACKNOWLEDGMENTS

We thank Professor L. Cederbaum and Dr. P. Schmelcher for helpful discussions. P. P. would like to thank the Greek Scholarships foundation (IKY) for financial support.

APPENDIX

In this appendix we present the calculation of the $N(t)/N_0$ function in the case of the scattering off two static disks. Including in the phase space integration the momentum of the projectile we obtain

$$\frac{N(t)}{N_0}=\frac{1}{A}\int d^2x\int d^2p\,\Theta\left(\frac{l(\mathbf{x})}{p/m}-t\right), \tag{A1}$$

where $l(\mathbf{x})$ is the distance traveled by the projectile starting its trajectory at $\mathbf{x}$ with momentum $\mathbf{p}$, Θ is the theta function, and C is a normalization constant given by

$$C=\int\int d^2x d^2p. \tag{A2}$$

Using polar coordinates, the integral over momentum can be performed as follows:

$$\frac{N(t)}{N_0}=\frac{2\pi}{A}\int d^2x\int_0^{ml(\mathbf{x})/t} p\,dp=\frac{\pi m^2}{At^2}\int d^2x\,l^2(\mathbf{x}) \tag{A3}$$

leading to $N(t)/N_0\sim t^{-2}$.

[1] U. Smilansky, in *Chaos and Quantum Physics*, Les Houches Lecture Notes, edited by M. J. Giannoni *et al.* (North-Holland, New York, 1992).
[2] B. Eckhardt, Physica D **33**, 89 (1988).
[3] C. Jung and H.J. Scholz, J. Phys. A **20**, 3607 (1988).
[4] E. Ott and T. Tél, Chaos **3**, 417 (1993).
[5] J.V. José, C. Rojas, and E. Saletan, Am. J. Phys. **60**, 587 (1992).
[6] P. Gaspard and S. Rice, J. Chem. Phys. **90**, 2225 (1989).
[7] Y.C. Lai and C. Grebogi, Int. J. Bifurcation Chaos Appl. Sci. Eng. **1**, 667 (1991).
[8] Z. Lu *et al.*, Phys. Rev. A **45**, 5512 (1992); **60**, 587 (1992).
[9] L. Wiesenfeld, Phys. Lett. A **144**, 467 (1990); J. Phys. B **25**, 4373 (1992).
[10] N. Meyer *et al.*, J. Phys. A **28**, 2529 (1995).
[11] A.J. Fendrik and D.A. Wisniacki, Phys. Rev. E **55**, 6507 (1997).
[12] K. Alexandrou and I. Kyprianou, e-print, chao-dyn/9811018.
[13] Z. Neufeld and T. Tél, Phys. Rev. E **57**, 2832 (1998).
[14] A. Antillón, J. José and T.H. Seligman, Phys. Rev. E **58**, 1780 (1998).
[15] J. Mateos, Phys. Lett. A **256**, 113 (1999).
[16] Y.T. Lau, J.M. Finn, and E. Ott, Phys. Rev. Lett. **66**, 978 (1991).
[17] V. Constantoudis and C. Nicolaides, Phys. Rev. A **55**, 1325 (1997).
[18] P. Gaspard, *Chaos, Scattering and Statistical Mechanics* (Cambridge University Press, Cambridge, England, 1998).
[19] A. Brahic, Astron. Astrophys. **12**, 98 (1971).
[20] A.J. Lichtenberg and M.A. Lieberman, *Regular and Stochastic Motion* (Springer-Verlag, New York, 1983).